JOURNAL OF GEOPHYSICAL RESEARCH, VOL. 102, NO. B12, PAGES 27,305–27,317, DECEMBER 10, 1997

Effective elastic thickness of the lithosphere along the Easter Seamount Chain

Sarah E. Kruse

Geology Department, University of South Florida, Tampa

Zhengrong J. Liu[1] and David F. Naar

Marine Science Department, University of South Florida, St. Petersburg

Robert A. Duncan

College of Oceanic and Atmospheric Sciences, Oregon State University, Corvallis

Abstract. Bathymetry and gravity data collected during Legs 5, 6, and 7 of the 1993 GLORIA Expedition and the recently released 2-min altimetry-derived global gravity grid are used to determine the effective elastic thickness of the lithosphere along the Easter Seamount Chain (ESC). Forward modeling, admittance, and coherence methods yield consistent results. With the exception of the eastern and western ends of the ESC the effective elastic thickness along the chain is ~1-4 km. The thin elastic thickness for the majority of the ESC seamounts is compatible with a young seafloor age at the time of loading derived from new radiometric ages of the seamounts along the chain and a magnetic isochron age interpretation of the Nazca plate seafloor age. The elastic thickness southeast of the Nazca fracture zone is ~6 km, apparently because of the seafloor age discontinuity across the fracture zone. The elastic thickness near the San Felix Island, at the eastern end of the ESC, is even greater (~11 km), which is compatible with the estimated seafloor age at the time of loading. A slight increase in the effective elastic thickness of the far western part of the ESC suggests dynamic compensation or less thermal weakening of lithosphere above a plume channel versus directly above the plume center. These findings combined with published geochemistry support a hotspot origin for the ESC, complicated by large-scale plate boundary reorganizations and channeling of plume material to the East Pacific Rise.

1. Introduction

The Easter Seamount Chain (ESC) is a major bathymetric feature in the southeastern Pacific (Figure 1) and was initially named the Sala y Gomez ridge [*Fisher and Norris*, 1960; *Menard et al.*, 1964]. The chain extends from west to east approximately 3000 km across the Nazca plate. The Easter microplate and the fastest, shallowest spreading portion of the East Pacific Rise are located 100 km west of the western end of the ESC [*DeMets et al.*, 1990; *Hey et al.*, 1995; *Naar and Hey*, 1989, 1991]. The eastern end of the ESC joins the southwestern end of the Nazca ridge on the southeastern side of the Nazca fracture zone near the San Felix Island [*Pilger and Handschumacher*, 1981; *Liu et. al.*, Evolution of the southeast Pacific and Easter Seamount Chain, submitted to *Journal of Geophysical Research*, 1996 (hereinafter referred to as *Liu et al.*, submitted manuscript, 1996)].

A simple hotspot model was initially proposed to explain the origin of this chain [*Morgan*, 1971; *Wilson*, 1963a, b, 1965; *Pilger and Handschumacher*, 1981; *Okal and Cazenave*, 1985]. Alternative hypotheses have been advanced over the last several decades to explain the apparent contemporaneous volcanism along the ESC (based on K-Ar age data). These hypotheses include a "hot line" model, in which the ESC formed along a thermal anomaly corresponding to an upwelling limb of a secondary convection roll [*Bonatti and Harrison*, 1976; *Bonatti et al.*, 1977], a "leaky fracture zone" model [*Clark and Dymond*, 1977; *Herron*, 1972a, b], and a "diffuse extension" model in which the ESC originated along tension cracks [*Sandwell et al.*, 1995; *Winterer and Sandwell*, 1987].

Now that more accurate ^{40}Ar-^{39}Ar ages [*O'Connor et al.*, 1995; *Liu*, 1996; R. Duncan, unpublished data, 1996] show an overall general age progression eastward along the chain, models for contemporaneous volcanism will not be discussed further. The diffuse extension model [*Sandwell et al.*, 1995] predicts east-west oriented tension cracks which are not observed in the GLORIA-6 kHz side scan data [*Liu*, 1996; *Hey et al.*, 1995; *Rusby and Searle*, 1995], SeaMARC II 12-kHz side scan data [*Hagen et al.*, 1990; *Naar and Hey*, 1991] and the 12-kHz SeaBeam 2000 backscatter intensity data [*Liu*, 1996; *Hey et al.*, 1995]. A modified hotspot model [*Ihinger*, 1995] has been proposed to explain the en echelon age of progressive volcanic ridges (Plate 1) near the western end of the ESC [*Liu*, 1996]. The model suggests that a plume may rise in the form of a series of buoyant mantle blobs [*Schilling and Noe-Nygaard*, 1974] which are sheared, while rising, into football-shaped bodies. The western ESC volcanic ridges may be tapping such elongated mantle sources at the base of the lithosphere, although the

[1]Now at Computer Science Department, Stanford University, Palo Alto, California.

Paper number 97JB02158.
0148-0227/97/97JB-02158$09.00

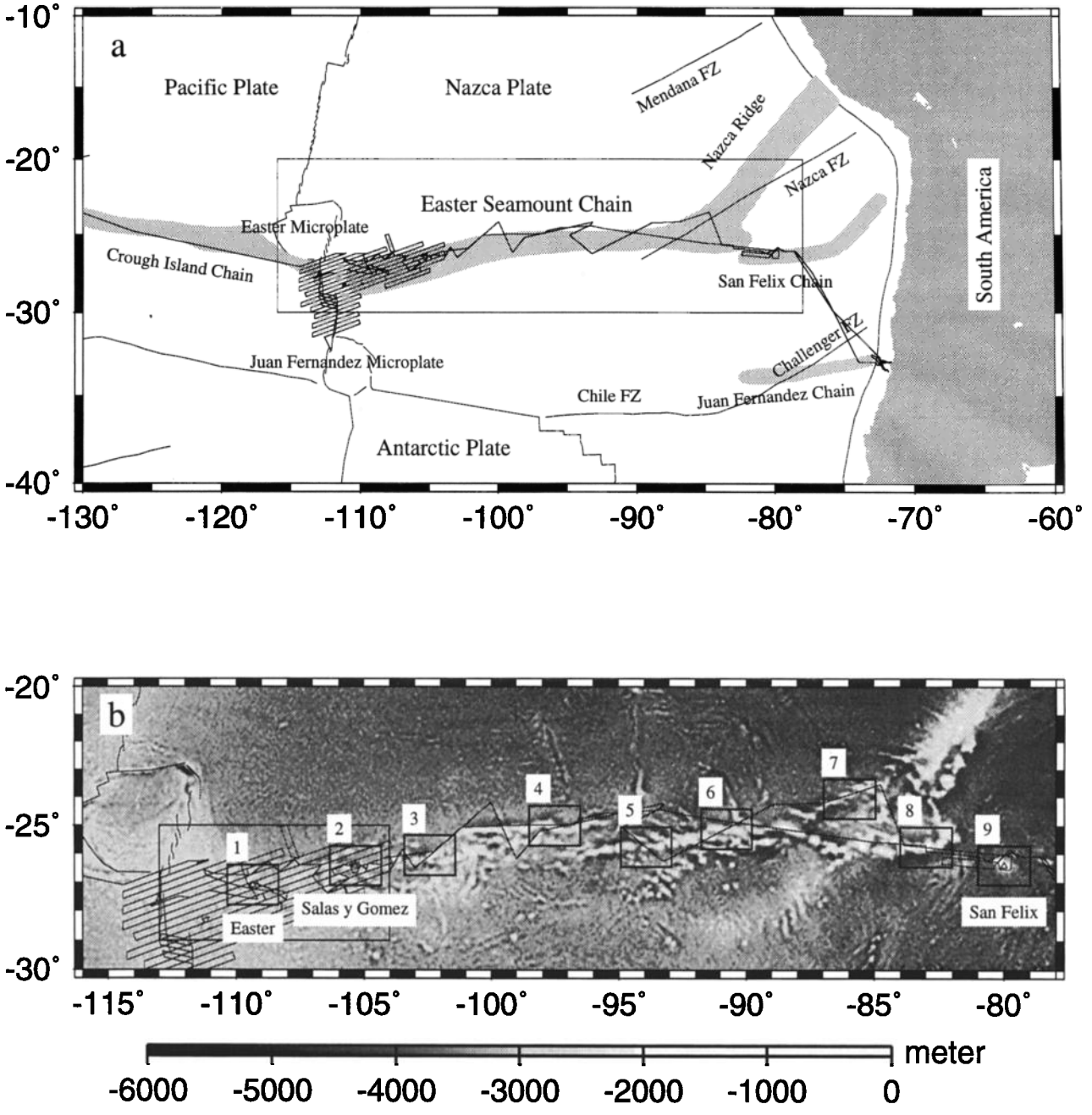

Figure 1. Tectonic setting and data. (a) Tectonic setting of the Easter Seamount Chain (ESC). The jagged line in the central region represents the ship tracks from Legs 5, 6, and 7 of the Gloria Expedition in 1993. Seamounts are indicated approximately by light stippled areas, although some volcanic flows extend to north or south of the stippled areas. Box shows the boundary of Figure 1b. (b) Bathymetry predicted [*Smith and Sandwell*, 1994; Liu et al., submitted manuscript, 1996] from ETOPO-5 data [*National Oceanic and Atmospheric Administration (NOAA)*, 1988] and gravity anomalies calculated from newly declassified altimetric data collected with Geosat/Exact Repeat Mission (ERM), Geosat/GM, ERS 1, and ERS 1/GM [*Smith and Sandwell*, 1995a, b]. Jagged line shows ship track as in Figure 1a. Numbered boxes show nine areas where T_e is modeled. Triangles mark locations of the islands along the ESC. Large box near western end shows location of Plate 1.

majority of the geochemical data only require that channeling occurs underneath the lithosphere [*Morgan*, 1978; *Schilling*, 1991] to the ridge axis from a hotspot somewhere near Salas y Gomez Island [*Kingsley et al.*, 1994; *Schilling et al.*, 1985; *Hanan and Schilling*, 1989; *Fontignie and Schilling*, 1991; *Schilling*, 1991; *Poreda et al.*, 1993a, b] or from somewhere farther west (closer to the ridge axis) [*Stoffers et al.*, 1994; *O'Connor et al.*, 1995; *Haase et al.*, 1996; *Haase and Devey*, 1996].

In this paper we use new bathymetry and gravity data and both forward modeling and spectral methods (admittance and coherence) to determine the effective elastic thickness of the lithosphere (T_e) supporting the ESC and San Felix Island. The integrated lithospheric strength can be expressed in terms of a

flexural rigidity, which can, in turn, be related to thickness of an elastic plate with flexural properties that approximate those of the lithosphere. Because this effective elastic plate thickness reflects the strength of the lithosphere at the time the seamounts form, it can be used as an indicator of thermal structure or age of the lithosphere at that time. Thus we can use estimates of T_e to test the predictions of the various models for the formation of the ESC and San Felix Island.

Both shipboard geophysical data [*Hey et al.*, 1995; *Naar et al.*, 1993a, b] and the new altimetry-based 2-min global gravity grid [*Smith and Sandwell*, 1995a, b] are independently used to estimate T_e. Shipboard data include swath bathymetry and gravity collected along the ESC during Legs 5, 6, and 7 of the 1993 GLORIA Expedition [*Hey et al.*, 1995; *Naar et al.*, 1993b]. In this paper, gravity data collected along the ship tracks of the GLORIA Expedition are referred to as shipboard gravity, while the new global gravity grid is referred to as altimetry gravity. We use a high-resolution grid of bathymetry data (node spacing of ~300 m) which has been compiled along the ESC [*Z. J. Liu and D. F. Naar*, Swath bathymetry processing of GLORIA-B and SeaBeam 2000, submitted to Marine Geophysical Researches, 1997 (hereinafter referred to as *Liu and Naar*, submitted manuscript, 1997)]. The data include the bathymetry swaths collected with both GLORIA-B and SeaBeam 2000 systems with swath widths of ~24 and ~10 km, respectively. Outside the coverage of the bathymetry swaths the bathymetry grid is filled with the ETOPO-5 data set [*National Oceanic and Atmospheric Administration*, 1988]. Near the Easter and Salas y Gomez islands (Plate 1), bathymetry values along the ~6 km gaps between the GLORIA-B swaths are interpolated from both GLORIA-B and SeaBeam swaths (Plate 1a).

We estimate the best fitting elastic plate thicknesses over several regions along the ESC and near San Felix Island. The models described above for the formation of the ESC differ in their predictions of the effective elastic thickness of lithosphere along the seamount change. To discriminate between these models, we determine T_e at nine distinct areas that span the ESC. These areas are shown as boxes 1 through 9 in Figure 1. We then turn to westernmost portion of the ESC, the Easter-Salas y Gomez region shown in Plate 1. As stated above, it has been postulated that the plume responsible for the ESC underlies this region. To assess possible effects of the plume on lithospheric strength in this region, we estimate T_e in five subregions with excellent shipboard bathymetry coverage. These subregions correspond to boxes a through e in Plate 1a.

2. Methods

To determine best fitting T_e values, we turn to a combination of forward, admittance, and coherence methods. Each method ultimately yields a T_e estimate from the relationship between seafloor bathymetry and gravity, which is measured at the sea surface or derived from satellite altimetry. Topographic loads on the seafloor are assumed to be isostatically compensated at the Moho by flexure of a lithosphere with a uniform effective elastic thickness. A greater effective elastic thickness implies a stronger plate, which flexes with a longer wavelength to support a given topographic load. Gravity anomalies observed at the sea surface are sensitive to both the topographic loads and to the deflections of the Moho. The relationship between the topographic loads and underlying Moho deflections, as well as the gravity response to each, can be described relatively simply in the Fourier domain. Free-air gravity anomalies expected for lithosphere with a specified T_e are calculated from bathymetry data using the relationship between the Fourier transform of the bathymetry and the Fourier transform of the resulting gravity anomaly:

$$\Delta G_f(k) = 2\pi\Delta\rho_0 G(-e^{-kz_m}/\zeta + e^{-kz_c})H(k), \quad (1)$$

where $\Delta G_f(k)$ is the Fourier transform of the free-air gravity anomaly, $H(k)$ is the Fourier transform of the bathymetry, k is wave number, $\Delta\rho_o$ is crustal density-water density, G is the gravitational constant, z_m is Moho depth, z_c is seafloor depth and,

$$\zeta = 1 + Dk^4/\Delta\rho_1 g, \quad (2)$$

where D is flexural rigidity, $\Delta\rho_1$ is mantle density-crustal density, and $g = 9.8$ m/s^2. The flexural rigidity D is related to the effective elastic plate thickness T_e via

$$D = \frac{ET_e^3}{12(1-\nu^2)}, \quad (3)$$

where E is Young's modulus and ν is Poisson's ratio. The first term in the parentheses of (1) yields the gravity signal related to the flexure of the Moho. T_e is incorporated into this term, as the wavelengths of the flexure reflect the effective elastic plate thickness. We use a constant crustal thickness (z_m-z_c) of 7 km, compatible with the results of a study using the group velocity of fundamental mode Rayleigh waves [*Woods and Okal*, 1994].

2.1. Forward Modeling Method

With the forward modeling method, shipboard gravity measurements are compared directly with theoretical gravity anomalies computed via (1) using the observed bathymetry. An inverse Fourier transform of the gravity predicted by (1) yields "model" gravity anomalies for a given T_e over the grid, which are then interpolated to the ship track locations. The model gravity anomalies are compared to the data for a range of values of T_e and crustal density. The other parameters in (1) - (3) (crustal density, mantle density, seafloor depth, and Moho depth) have a much smaller effect on the model gravity and are held fixed at the values listed in Table 1. The best fitting T_e value for a given region is defined as that for which the root mean square (RMS) difference between model gravity and data is a minimum, as in *Wolfe and McNutt* [1991]. Uncertainties in T_e are calculated using a standard χ^2 method and other estimates of systematic errors. Figure 2 shows an example of observed and forward model gravity across the Easter and Salas ridges, along the ship track indicated by the white line in Plate 1b.

2.2. Admittance Method

The effective elastic plate thickness can also be estimated by comparing the observed gravity anomalies and the bathymetry in the Fourier domain. For a lithosphere of uniform T_e the admittance function, or ratio of the Fourier transform of the gravity to the Fourier transform of the bathymetry, can be derived from (1) as

$$F(k) = \Delta G_f(k)/H(k) = 2\pi\Delta\rho_0 G(-e^{-kz_m}/\zeta + e^{-kz_c}) \quad (4)$$

[e.g., *Dorman and Lewis*, 1970; *Banks et al.*, 1977; *McNutt*,

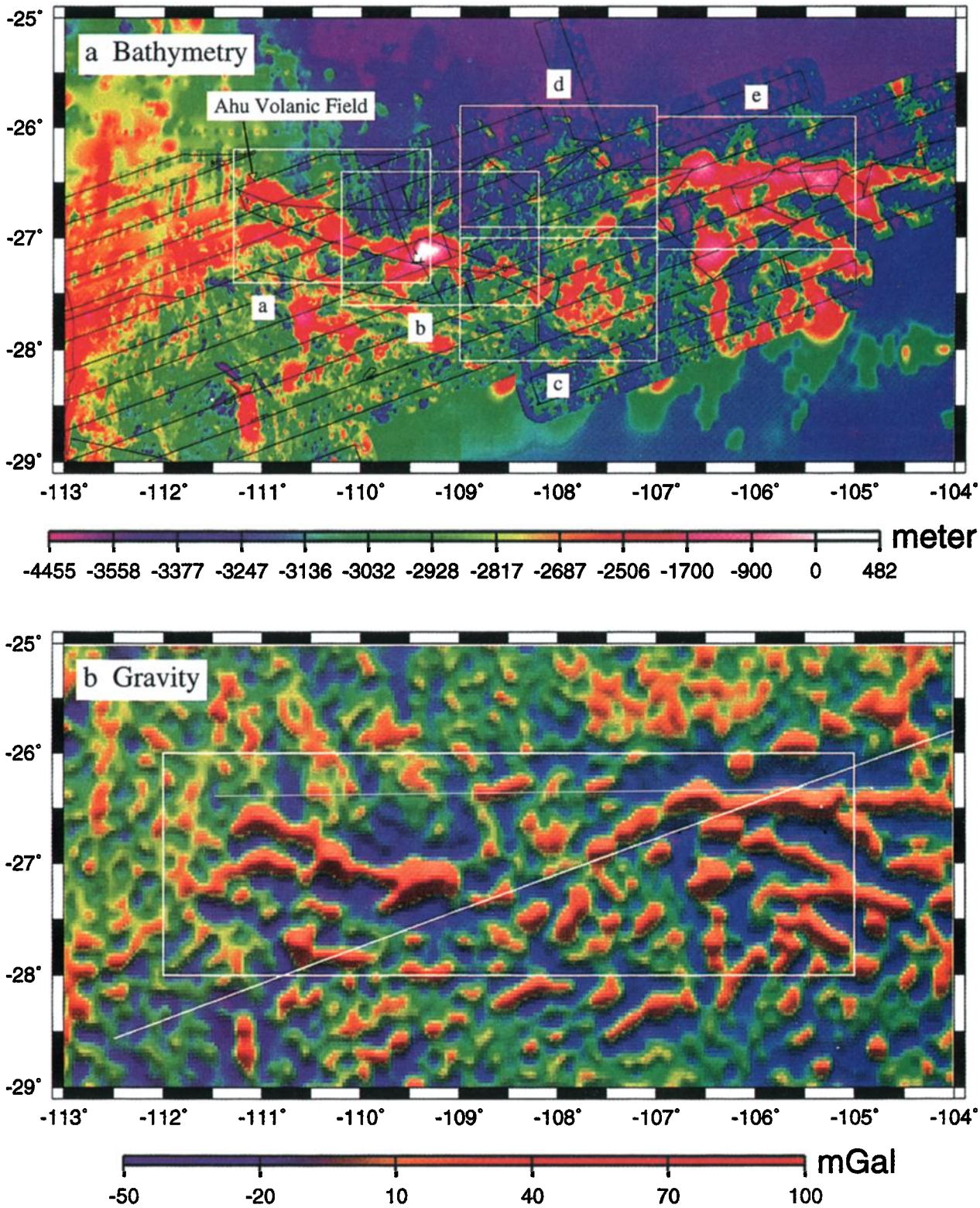

Plate 1. Easter-Salas y Gomez region. Location shown in Figure 1b. (a) Bathymetry data compiled from swath bathymetry data collected during the Gloria Expedition using both GLORIA-B and SeaBeam systems [Liu and Naar, submitted manuscript, 1997]. Outside of the survey region west of 109°W, data are from F. Martinez [personal communication, 1995]; east of 109°W, data are from ETOPO-5 [*NOAA*, 1988]. Black line shows ship track. Boxes show subareas where T_e is modeled. (b) Gravity anomaly in Easter-Salas y Gomez region from the 2-min global gravity grid [*Smith and Sandwell*, 1995a, b]. T_e is modeled with admittance and coherence methods in box. Diagonal line represents the profile shown in Figure 2.

Table 1. List of Default Values of Physical Parameters

Parameter	Definition	Value
E	Young's modulus	7×10^{10} N/m^2
ν	Poisson's ratio	0.25
G	gravitational constant	6.67 x 10-11 m^3/s^{2}kg
g	gravitational acceleration	9.8 m/s^2
$\Delta\rho_0$	crust-water density contrast	1600 kg/m^3
$\Delta\rho_1$	mantle-crust density contrast	550 kg/m^3
ρ_w	density of seawater	1030 kg/m^3
z_c	seafloor depth	3 km
z_m	Moho depth	10 km
T_e	effective elastic plate thickness	3 km
f	weighted subsurface/surface load ratio	0

1980; *Louden and Forsyth*, 1982]. Parameters are defined as in (1) - (3). The admittance function defined in (4) assumes all loads on the plate are topographic, neglecting possibly significant subsurface loads. Following *Forsyth* [1985], (4) can be modified to incorporate the effects of subsurface loads. Here we assume that all such subsurface loads lie at the Moho. The relative amplitude of subsurface loads can be introduced with the parameter f, which defines the ratio of the subsurface load at the Moho to the surface topographic load.

$$f = \frac{\Delta\rho_1 H'\zeta}{\Delta\rho_0 H}.$$

Here H' is the Fourier transform of the topography that develops in response to the subsurface load. To describe the flexure in response to subsurface loads, a new parameter ϕ is needed, where

$$\phi = 1 + Dk^4 / \Delta\rho_0 g$$

The expanded expression for the admittance becomes

$$F(k) = -2\pi\Delta\rho_0 G\left[\frac{\phi f^2 \Delta\rho_0^2 + \zeta\Delta\rho_1^2}{f^2\Delta\rho_0^2 + \zeta^2\Delta\rho_1^2} e^{-kz_m} + e^{-kz_c}\right]. \quad (5)$$

Figure 3 shows admittance curves predicted using (5) as a function of the model parameters. The location and amplitude of the central peak in the admittance curves are particularly sensitive to both T_e and f (Figures 3a and 3b). On a stiffer plate (higher T_e) the wavelength of Moho deflections compensating bathymetric loads increases, producing a longer wavelength gravity signal (Figure 3a). Differences in T_e are distinguished principally at wavelengths between 50 and 200 km. We find that the altimetry gravity is coherent with shipboard gravity at

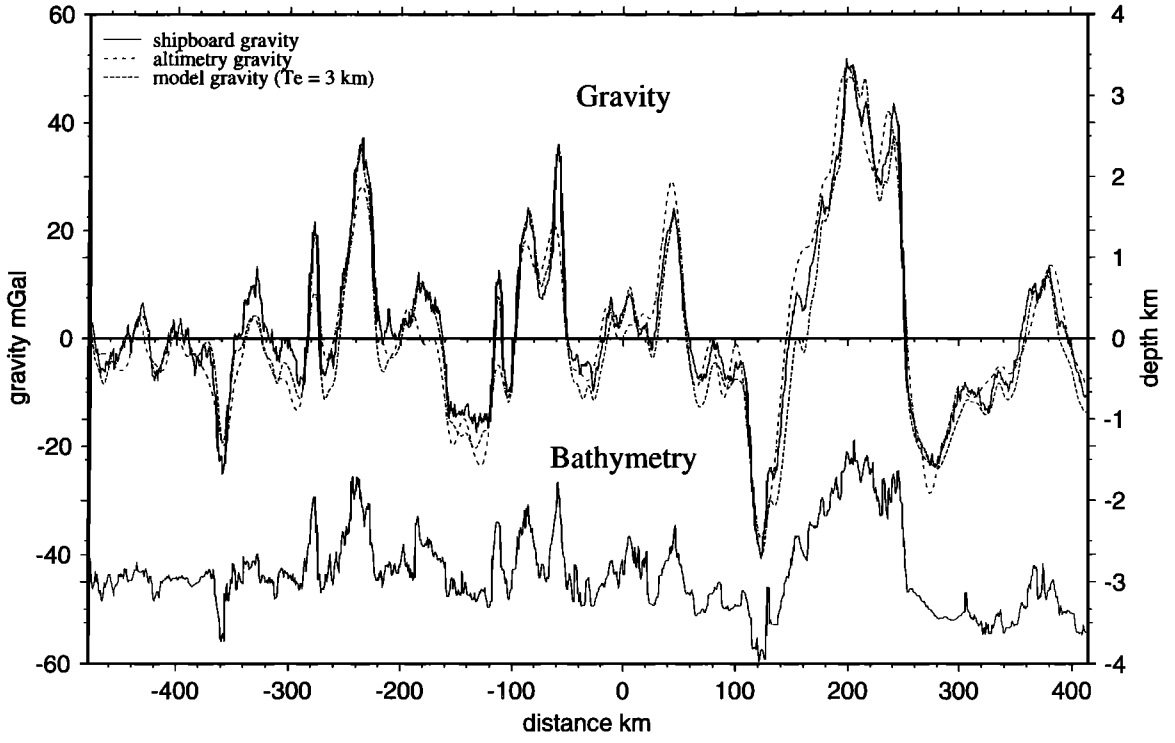

Figure 2. Gravity and bathymetry along the profile indicated by the white line in Plate 1b. Altimetry gravity is interpolated along the ship track. Synthetic gravity is modeled from two-dimensional bathymetry data assuming T_e = 3.0 km. Shipboard gravity and SeaBeam 2000 bathymetry data were collected during Legs 5 and 6 of the Gloria Expedition.

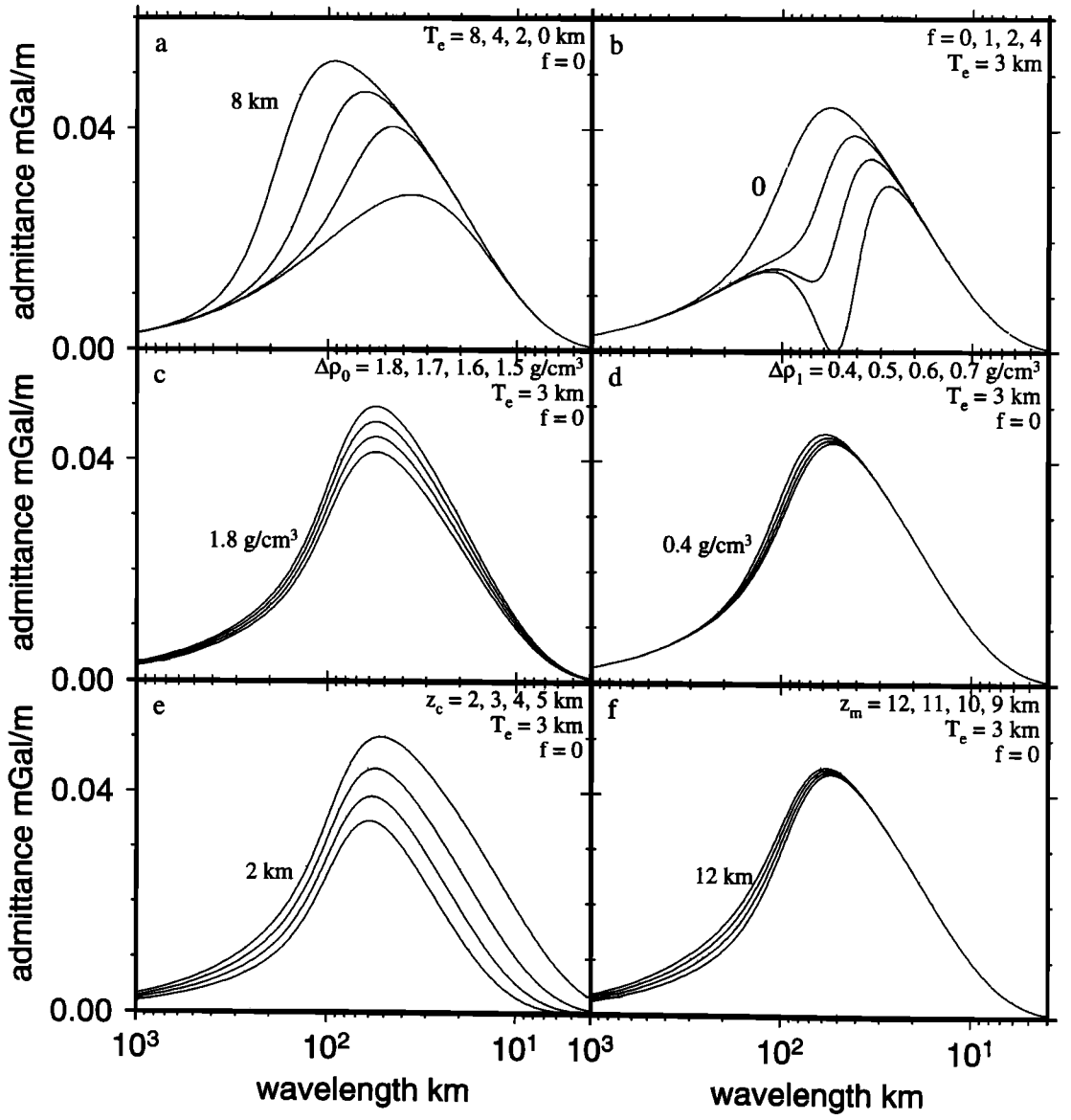

Figure 3. Theoretical admittance curves as a function of (a) elastic plate thickness, (b) loading parameter, (c) crust-water density contrast, (d) mantle-crust density contrast, (e) seafloor depth, and (f) depth to Moho. Default values for parameters not listed with each graph are shown in Table 1.

wavelengths greater than approximately 50 km, as expected from the resolution of altimetry gravity [*Smith and Sandwell*, 1995a, b]. Thus it appears reasonable to use altimetry gravity with the admittance method. Variations in other model parameters have smaller effects on the admittance (Figures 3c-3f).

The observed admittance values are computed for two-dimensional grids using the bathymetry data described above and the altimetry gravity grid. Grid size is set through a compromise of (1) sampling wavelengths long enough to capture the peak in the admittance curve and (2) restricting the study area to a limited tectonic province. In a large region, admittance may place primary emphasis on the areas with the greatest topographic relief [*Forsyth*, 1985]. To avoid bias by noise, the admittance values of the observed data are computed in practice as

$$\hat{F}(k) = \frac{\langle \Delta G_f(k) \cdot H^*(k) \rangle}{\langle H(k) \cdot H^*(k) \rangle},$$

where angle brackets indicate an average over discrete wave number bands and asterisks indicate the complex conjugate. The observed admittance values are then compared to model curves for various values of T_e and f.

2.3. Coherence Method

In practice, with the admittance method it may be difficult to simultaneously resolve both T_e and f (subsurface/surface load ratio). An alternative method, the coherence method, can assess T_e with much less sensitivity to f [*Forsyth*, 1985]. In this method, T_e is estimated from the coherence rather than the ratio of the Fourier transforms of the gravity and bathymetry. The coherence γ^2 is defined as

$$\gamma^2 = \frac{C^2}{E_0 E_1},$$

where E_0, E_1, and C are the power of bathymetry and gravity and the cross power between them, respectively [*Forsyth*, 1985].

For a given T_e the theoretical coherence can then be computed using Bouguer gravity anomalies as

$$\gamma^2 = \frac{(\zeta\Delta\rho_1^2 + \phi f^2\Delta\rho_0^2)^2}{(\zeta^2\Delta\rho_1^2 + f^2\Delta\rho_0^2)(\Delta\rho_1^2 + \phi^2 f^2\Delta\rho_0^2)}. \quad (6)$$

The coherence method assumes that surface and subsurface loads are statistically independent [*Forsyth*, 1985]. If they are, in fact, strongly correlated, there is a downward bias in T_e estimates [*Macario et al.*, 1995]. However, observations suggest that these loads are generally not strongly correlated [*Forsyth*, 1985; *Macario et al.*, 1995]. On the other hand *Macario et al.* [1995] show that there may be an upward bias in T_e values if the grid used is too small to capture the longest wavelengths. To avoid the latter bias, we compute coherence over a large grid.

3. Results

3.1. Along the ESC and Near San Felix Island

T_e is estimated for nine distinct areas that span the ESC (Figure 1b). The western eight (areas 1-8) lie along the ESC, while the easternmost one (area 9) is near San Felix Island. Area 7 is near or on the Nazca fracture, while area 8 is across the fracture zone on the same side with San Felix Island (Figures 1a and 1b). On these nine grids, shipboard bathymetry data are limited to swaths ~24 km wide. Outside of the swaths the grid is filled with ETOPO-5 bathymetry, as described above. Because of the poor quality of the ETOPO-5 bathymetry, we use only the forward modeling method on these grids. The forward modeling method has the advantage of fitting gravity data only along the ship tracks, unlike the admittance and coherence methods which weight data throughout the grid equally. The remaining uncertainties associated with the errors in ETOPO-5 bathymetry are discussed further below.

The results of forward modeling are shown in Figure 4 and Table 2. Figure 4 shows contours of the RMS difference between the model and shipboard gravity in each area for a range of values of crustal density and elastic plate thickness. Lighter gray indicates smaller RMS values. The patterns of RMS contours show that best fitting T_e values are generally fairly well constrained despite uncertainties in crustal densities. For a crustal density of 2650 kg/m^3 the best fitting T_e values are 3.4, 2.6, 2.2, 4.2, 1.6, 3.4, 3.2, 7.8, and 8.2 km for areas 1-9, respectively.

To estimate the uncertainty in the T_e values, we computed χ^2 uncertainties for the T_e and crustal density grids shown in Figure 4. For the χ^2 calculation, we assume a standard deviation of 5 mGals in the shipboard gravity measurements made with the Bell Gravity Meter Version 3 aboard the R/V *Melville*. This value lies below the global standard deviation of ~14 mGals [*Wessel and Watts*, 1988] but above the ~0.4 mGal capabilities of this modern instrument under ideal conditions [*Bell and Watts*, 1986]. The number of data points used in computing the RMS difference between observed and model gravity in each of the nine areas is very large (the number ranges from 630 to 5062). As a result, the χ^2 uncertainties, which assess the contribution of random errors to the uncertainty in T_e, are quite small, less than 0.4 km. The observation that the RMS minima are found out of the range of several of the grids shown in Figure 4, at unrealistically high or low crustal densities, suggests that systematic errors dominate uncertainties in T_e. The limitations of the model certainly include the assumptions that T_e and the crustal density are uniform throughout the modeled region, that all lithospheric loads are topographic, and that all compensation of loads occurs at the Moho. To assess of the goodness of fit of the T_e values more realistically, we find the range of T_e values where the RMS fit is within 5% of the minimum value. This range corresponds well with uncertainties estimated from visual inspections of forward modeling ship track profiles.

Errors associated with the poor quality of the ETOPO-5 bathymetry introduce additional uncertainties in the estimate of

Table 2. Effective Elastic Plate Thickness Estimated Along the ESC and in the Easter-Salas y Gomez Region

Area	Age,* m.y.	T_e,† km fixed ρ_c	T_e,†† km	Tectonic Site
1	4±2	3.4	4.1±1.4	Easter Island on pseudofault
2	4±2	2.6	3.2±1.6	Salas y Gomez Island on normal seafloor
3	4±2	2.2	2.6±2.6	seamount on normal seafloor
4	5±2	4.2	3.2±2.3	seamount on normal seafloor
5	1±2	1.6	1.4±1.4	seamount near Mendoza rift
6	4±2	3.4	3.2±2.0	seamount on normal seafloor
7	1±2	3.2	3.0±2.9	seamount on Nazca fracture zone
8	8±2	7.8	5.9±1.9	seamount on older seafloor southeast of Nazca fracture zone
9	30±2	8.2	10.6±2.9	San Felix Island on older seafloor southeast of Nazca fracture
a	4±2	4.2	4.5±1.9	Ahu Volcanic Field and part of Easter Island
b	4±2	4.0	4.7±2.8	Easter Island
c	4±2	2.0	2.0±1.2	Easter Ridge between Easter Island and Salas y Gomez Island
d	4±2	1.6	1.8±1.0	between Easter Island and Salas y Gomez Island
e	4±2	2.4	2.8±0.6	Salas y Gomez Island and Ridge

*Age of seafloor at time of seamount formation.

†Best-fitting T_e value assuming crustal density of 2650 kg/m^3.

††Range of values = range over which RMS misfit between observed and model gravity is within 5% of RMS minima in the grids shown in Figures 5 and 7. In regions 1-9 an uncertainty of 1 km is added to the upper and lower limits to account for errors associated with using off-track ETOPO-5 bathymetry. See text for discussion.

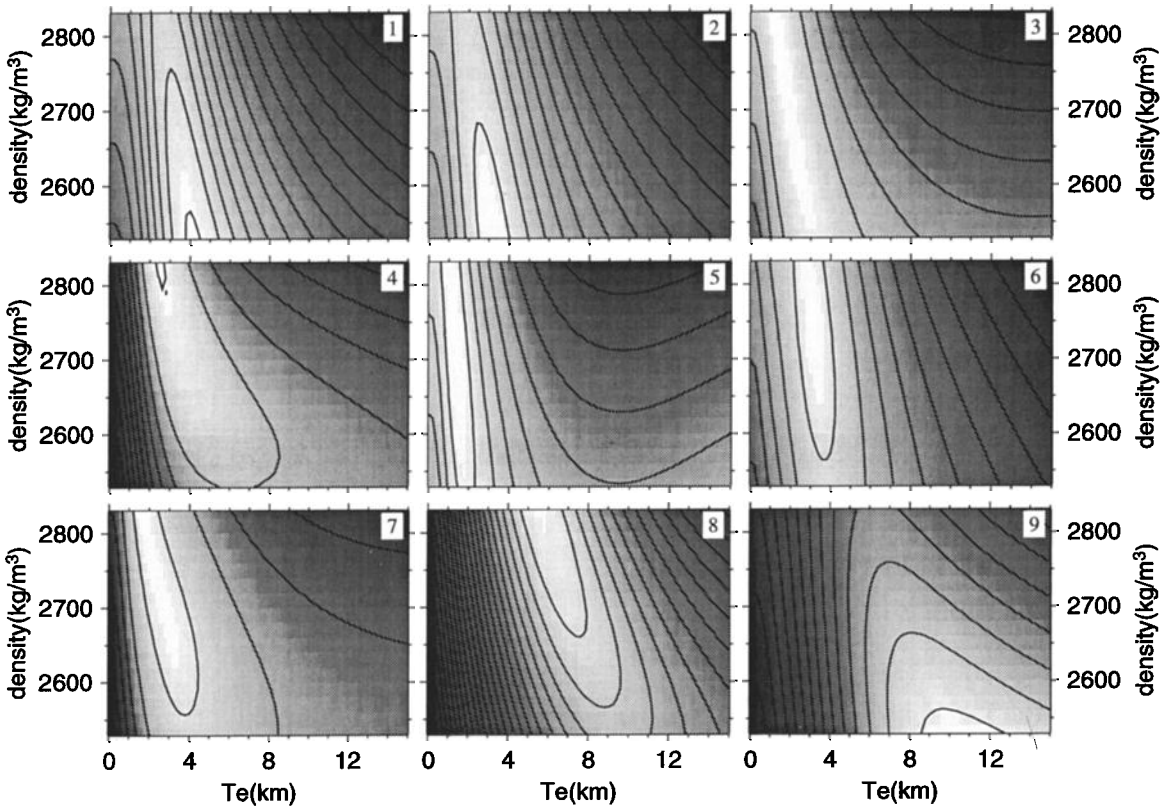

Figure 4. Forward modeling of T_e along the ESC. Panels 1 through 9 correspond to the nine areas in Figure 1b. Contours show the RMS difference between shipboard gravity and model gravity for a range of values of T_e and crustal density. Lighter gray indicates lower RMS values. RMS minima are 2.9, 3.6, 6.1, 6.9, 4.4, 6.6, 6.8, 5.2, and 4.7 mGals for grids 1-9, respectively. Contour interval is 1 mGal. Calculations were done varying T_e and crustal density by intervals of 0.2 km and 20 kg/m^3, respectively.

T_e. Along the ship tracks, ~20% of the theoretical gravity signal is derived from regions outside of the swath where bathymetry coverage is good. This number is valid for bathymetry variations of the order of 500 m and a bathymetry swath width of 24 km. To estimate the potential effect of bathymetry errors outside the swath, we computed RMS fits as described above, replacing all non shipboard bathymetry values with a constant value which was within 500 m of the maximum or minimum depth for the region. In this way we generate a long-wavelength bathymetry signal (long wavelengths contribute more strongly to gravity measured along the ship track than short wavelengths at comparable location). We modeled the effect of erroneous bathymetry in regions where T_e is relatively well constrained (region 5) and poorly constrained (region 9). The effect of the extreme false bathymetry is to shift the best fitting T_e values by up to 1.5 km from the minima shown in Figure 4. Actual errors associated with the ETOPO-5 bathymetry are probably considerably less than the errors introduced in this exercise. Thus we assume here that the uncertainty in T_e estimates associated with ETOPO-5 errors is of the order of +/- 1 km. Table 2 summarizes uncertainties for each region. The listed ranges of T_e values combine the ranges derived from the RMS grids as discussed above with an additional 1 km added to each end of the range to include the ETOPO-5 uncertainty.

3.2. Easter-Salas y Gomez Region

The western end of the ESC is dominated by several volcanic ridges (bathymetric highs on Plate 1a). With a nearly complete mosaic of swath bathymetry in this region (Plate 1a) we can use admittance and coherence methods, as well as the forward modeling method to determine T_e. We initially apply both admittance and coherence methods over a region encompassing most of the volcanic ridges (box in Plate 1b). This large grid minimizes the bias in coherence discussed above as well as errors that arise when modeling wavelengths of the order of the grid dimensions. The results, shown in Figure 5, indicate the best fitting regional value for T_e is ~3 km.

The coherence plots (Figures 5c and 5d) show the transition from high to low coherence takes place over a broader range of wavelengths than does the model for any specific elastic plate thickness (Figure 5c). This pattern may result from averaging over regions with different flexural rigidities. Considering uncertainties in f, the estimate of an elastic plate thickness of 3 km using the coherency method (Figures 5c and 5d) appears accurate to within ~1 km. The results of the admittance analysis (Figures 5a and 5b) suggest that subsurface loads are substantially less than surface loads (f < ~0.5). The consistent results from the coherence and admittance methods imply that a no subsurface load (f =0) assumption, which we use in the admittance modeling discussed below, introduces errors of less than ~1 km in estimates of T_e.

To look for potential variability in T_e within the Easter-Salas y Gomez region, we examine the five subareas a through e on Plate 1a. Coherence methods are found to be extremely noisy with these smaller grid sizes. Forward modeling of shipboard gravity throughout each of the subareas produces the results shown in

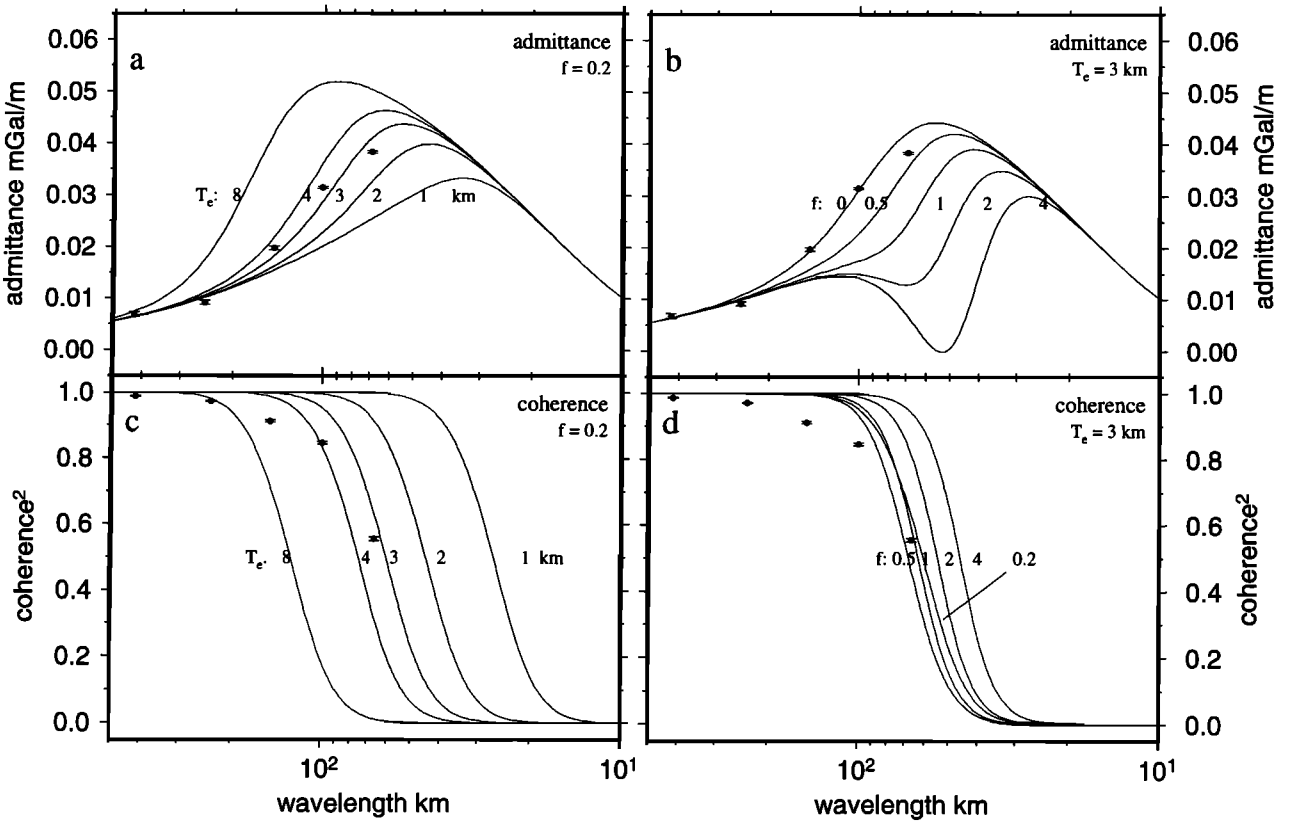

Figure 5. Admittance and coherence models for box shown in Plate 1b. Data values are computed using altimetry gravity and bathymetry grids. (a) Admittance as a function of T_e with fixed f. (b) Admittance as a function of f with fixed T_e. (c) Coherence as a function of T_e with fixed f. (d) Coherence as a function of f with fixed T_e. Coherence between the bathymetry and Bouguer gravity is calculated using equation (6) with an assumed crustal density of 2650 kg/m^3.

Figure 6. Assuming a crustal density of 2650 kg/m^3, the best estimates of T_e from minimizing the RMS misfit between model and data are 4.2, 4.0, 2.0, 1.6, and 2.4 km for subareas a-e, respectively. Admittance modeling of the bathymetry mosaic and the altimetry gravity grid in these sub-areas shows a similar pattern in T_e (Figure 7): a best fitting value of ~4 km is found in subareas a and b, while a value of ~2.5 km is found in subareas c-e. Uncertainties in T_e values are calculated from the forward modeling as for regions 1-9 above (Table 2). In the Easter-Salas y Gomez region, however, shipboard bathymetry coverage is nearly complete, so errors associated with ETOPO-5 bathymetry are negligible.

4. Discussion

4.1. Along the ESC and Near San Felix Island

The consistently low values of T_e (<5 km) found along the ESC are compatible with values obtained in previous satellite altimetry and seismic studies in this region [*Calmant*, 1987; *Woods et al.*, 1993]. These elastic thicknesses are slightly smaller than values of 4-8 km found on young seafloor near the Mid-Atlantic Ridge from coherence analysis [*Blackman and Forsyth*, 1991]. However, lithospheric reheating at the time of seamount or ridge emplacement may reduce the flexural rigidity of the lithosphere. Figure 8 shows the relationship between elastic plate thickness, isotherms, and seafloor age at time of loading for the ESC and for other seamounts formed on young lithosphere. Time of loading is computed by subtracting interpolated published and unpublished radiometric ages [*O'Connor et al.*, 1995; R. Duncan, unpublished data, 1996] from seafloor ages estimated from magnetic isochrons [*Liu*, 1996].

These data show that the majority of the seamounts were formed on seafloor younger than ~10 Ma and that at the western end of the chain the time of loading varies from about 9 Ma near 102°W (east of Salas y Gomez Island) to about 2 Ma near 111°W (western edge of the Ahu Volcanic Field) [Liu et al., submitted manuscript, 1996]. This time-of-loading pattern suggests that the "hotspot" volcanism has approached the seafloor spreading axis, which is contrary to Nazca-hotspot plate motion models which predict that the ridge should have migrated west from the Easter hotspot at about 20 mm/yr [*Minster and Jordan*, 1978; *Naar and Hey*, 1989; *Gripp*, 1994]. This implies that either the Nazca-hotspot motion is incorrect, that the Easter hotspot is not fixed and has moved toward the west at a rate greater than about 20 mm/yr, or that young volcanoes have formed over a "leaky" channel that has fed enriched "hotspot" mantle from the Easter hotspot to the Pacific-Nazca ridge axis [*Haase and Devey*, 1996; *Haase et al.*, 1996; *Hagen et al.*, 1990; *Hey et al.*, 1995; *Liu et al.*, 1995; *Lonsdale*, 1989; *O'Connor et al.*, 1995; *Okal and Cazenave*, 1985; *Pilger and Handschumacher*, 1981; *Schilling et al.*, 1985a, b; *Searle et al.*, 1995; *Stoffers et al.*, 1994; Liu et at., submitted manuscript, 1996; Z. J. Liu and D. F. Naar, Formation of the Easter Seamount Chain and implications for deep earth structure, submitted to *Journal of Geophysical Research*, 1997].

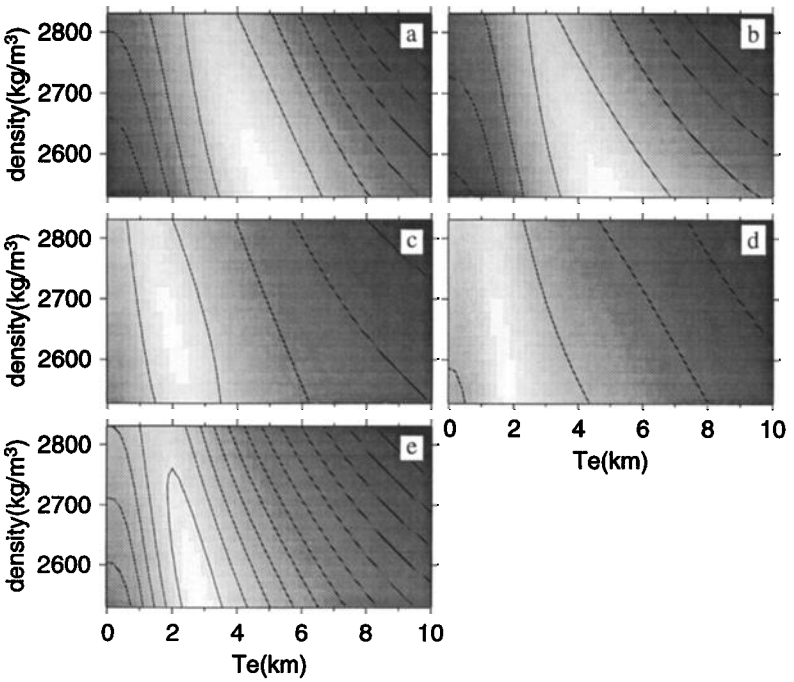

Figure 6. Forward modeling of T_e in Easter-Salas y Gomez region. (a)-(e) Areas a-e in Plate 1a. Contours show the RMS difference between shipboard gravity and model gravity for a range of values of T_e and crustal density. Lighter gray indicates lower RMS values. RMS minima are 9.4, 12.6, 2.8, 3.5, and 3.5 mGals for Figures 6a-6e, respectively. Contour interval is 1 mGal. Calculations were done varying T_e and crustal density by intervals of 0.2 km and 20 kg/m^3, respectively.

A leaky channel is very similar to the second type of hotspot island model [*Morgan*, 1978] except that instead of just channeling enriched mantle from the hotspot to the ridge axis, enriched mantle would also rise to form volcanoes wherever the lithospheric structure permits. The volcanoes that form by this process will be younger than predicted by the classic hotspot model but older than the *Morgan* [1978] model, which predicts the volcanoes would form at the ridge axis and thus would have the same age as the seafloor. In addition, a scatter of the seamount ages and time of loading is expected in this leaky channel model, because the volcanoes can form anywhere above the channel that the lithospheric structure permits. The general scatter and younger than expected radiometric ages of the enriched seamounts give support for this leaky channel model [*Liu*, 1996; *O'Connor et al.*, 1995], but we cannot rule out that the Easter hotspot is moving or that both processes have formed the time-of-loading pattern observed.

The relatively low T_e value estimated in area 7 (~3 km) may be due the weakness of the lithosphere near or on the Nazca fracture zone. The higher T_e values for the easternmost two areas (8 and 9) suggest loads formed on stronger, presumably older seafloor in this region. The ~6 km T_e estimate in area 8 supports this conclusion, as the Nazca fracture zone separates this older seafloor from the younger seafloor to the west along the ESC.

The high T_e value found near San Felix Island (area 9, Figure 1b) is also from the older side of the Nazca fracture zone. A young radiometric age (~0.8 Ma) [R. Duncan, unpublished data, 1996] and very recent volcanic activities in 1922 [*Firth*, 1943] indicate a much older seafloor age at time of loading than any of the other volcanoes along the ESC. There is also a gap of volcanoes between the ESC and San Felix Island [*Liu*, 1996; *Naar et al.*, 1993a, b]. The style of volcanism [*Liu*, 1996] and geochemical patterns [*Gerlach et al.*, 1986] are different between the ESC and San Felix Island. Finally, the general overall backscatter intensity of the GLORIA side scan images of young volcanism decreases along the ESC to the east but jumps to a high value near the San Felix Island [*Liu*, 1996]. Thus the higher T_e values are consistent with the interpretation that San Felix Island was not formed by the same process that formed the volcanoes along the ESC [*Gerlach et al.*, 1986; *O'Connor et al.*, 1995].

4.2. Easter-Salas y Gomez Region

Most elastic plate thickness estimates for seafloor loaded by seamounts lie in the depth range of the 200° to 500°C isotherms of the cooling lithosphere [*Wessel*, 1992]. Thus the ESC lithospheric strength falls within the broad range of values observed near other seamounts. However, the time-of-loading variation would predict that T_e should decrease toward the spreading axis. Instead, in the Easter-Salas y Gomez region on the westernmost ESC we see consistently lower best fitting T_e values in subareas c, d, and e (1.6-2.4 km) and an unexpected increase to 4.0-4.2 km in subareas a and b which are closest to the spreading axis. This difference in T_e values is seen in both forward modeling and admittance methods (Figures 6 and 7). While the uncertainties in T_e values of subareas a and b and c-e do overlap (Table 2), this overlap reflects primarily uncertainty in the crustal density and the trade off between density and T_e in the models. This suggests to us that there is (1) a higher crustal density in subareas a and b (which we have no reason to suspect), (2) some dynamic compensation which is giving an overestimation of T_e in areas a and b [*Blackman and Forsyth*, 1991], possibly related to upwelling associated with a "mantle

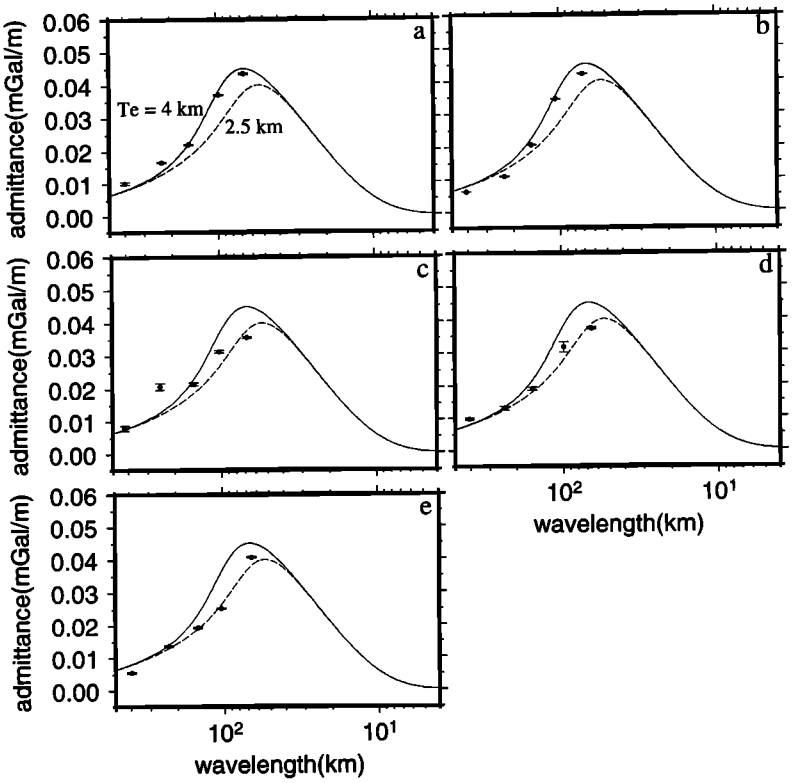

Figure 7. Admittance modeling of T_e for subareas a-e as in Figures 6a-6e. Circles show admittance data calculated from altimetry gravity and bathymetry grids; curves are admittance models. Models assume $f = 0$. Admittance solutions for area c as shown in Plate 1a were noisy because of a strong signal at wavelengths near the box dimension. Data shown here for the c grid are for a grid that extends 0.3° farther east and west than the box c shown.

channel", and/or (3) thermal weakening of the lithosphere east of boxes a and b perhaps related to the hotspot being located near Salas y Gomez Island. Although we have no way to constrain these possibilities, the latter is most compatible with the observed geochemical and age patterns [*Kingsley et al.*, 1994; *Schilling et al.*, 1985a; *Hanan and Schilling*, 1989; *Fontignie and Schilling*, 1991; *Poreda et al.*, 1993a]. Intuitively, one would expect lithosphere overlying a broad hotspot plume to be more

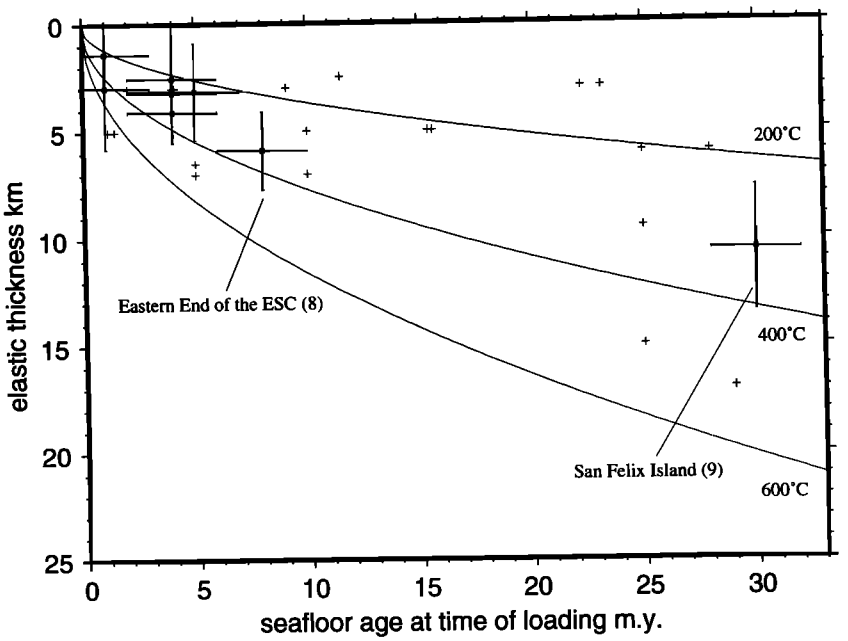

Figure 8. T_e versus age of seafloor at time of loading. Circles with error bars are data from this study. Error bars show uncertainties listed in Table 2. Small crosses represent data compiled by *Wessel* [1992] of seamounts from around the world (trench flexure data are excluded). Curves are isotherms for the cooling plate model [*Parson and Sclater*, 1977].

thermally weakened than lithosphere overlying a narrow channel supplying plume material to the ridge axis.

5. Conclusions

Together, the gravity analysis presented here and published geochemistry observations support a model in which the majority of the ESC is produced by a single hotspot combined with some tectonic complexities related to repeated large-scale plate boundary reorganizations and fracture zones crossing over the hotspot [*Liu*, 1996]. In general, the effective elastic plate thickness is found to be ~1-4 km along the western and central ESC, ~6 km on older seafloor east of the Nazca fracture zone, and ~11 km near the San Felix Island. Forward, admittance, and coherence methods with both shipboard and altimetry gravity data yield consistent results. Admittance and coherence methods together suggest that the weighted ratio of subsurface loads to surface loads f is less than 0.5.

T_e values along the chain lie between the 200° and 500°C isotherms for lithosphere at the time of loading, within the range observed in other studies of lithosphere loaded by seamounts. The T_e values are also consistent with other published geophysical and geochemical data pointing to a source and mode of formation of San Felix Island independent from that of the ESC. A locally slightly higher T_e value (4 km) at the far western end of the ESC between the Ahu Volcanic Field and Easter Island may reflect some kind of dynamic compensation or less thermal weakening of the lithosphere overlying the "plume channel" versus lithosphere overlying the hotspot plume farther to the east somewhere near Salas y Gomez Island.

Acknowledgments. We thank R. Hey for providing us with the bathymetry and gravity data collected during Leg 5 of the Gloria Expedition, F. Martinez for providing us with gridded bathymetry data near the Easter microplate, and R. Hagen for providing us with the digitized topographic data of Easter Island. Admittance and coherence were calculated with a slightly modified version of a program provided by D. Forsyth and G. Neumann, and χ^2 uncertainties we calculated with a program from U.E. Kruse. We thank D. Forsyth, G. Neumann, and W. Smith for useful comments. We also thank Y. Rappaport and M. Kuykendall for reviewing earlier drafts of this paper. Constructive reviews by G. Neumann, C. Wolfe, and Associate Editor J. Goff greatly improved the manuscript. This manuscript is revised from a chapter of the dissertation submitted by Z. J. Liu in partial fulfillment of the requirements for the Ph.D. degree at the University of South Florida. All figures were generated using Generic Mapping Tools (GMT) [*Wessel and Smith*, 1991]. Funding was provided by NSF grants OCE9116012, OCE9214494, OCE9214495, OCE9214496, OCE9258626, and OCE9302802.

References

Banks, R. J., R. L. Parker, and S. P. Huestis, Isostatic compensation on a continental Scale: Local versus regional mechanisms, *Geophys. J. R. Astron. Soc.*, *51*, 431-452, 1977.

Bell, R., and A. B. Watts, Evaluation of the BGM-3 sea gravimeter system on board R/V *Conrad*, *Geophysics*, 51, 1480-1493, 1986.

Blackman, D. K., and D. W. Forsyth, Isostatic compensation of tectonic features of the Mid-Atlantic Ridge: 25-27°30'S, *J. Geophys. Res.*, *96*, 11741-11758, 1991.

Bonatti, E., and C. G. A. Harrison, Hot lines in the Earth's mantle, *Nature*, *263*, 402-404, 1976.

Bonatti, E., C. G. A. Harrison, D. E. Fisher, J. Honnorez, J. G. Schilling, J. J. Stipp, and M. Zentilli, Easter Volcanic Chain (Southeast Pacific): A mantle hot line, *J. Geophys. Res.*, *82*, 2457-2478, 1977.

Calmant, S., The elastic thickness of the lithosphere in the Pacific Ocean, *Earth Planet. Sci. Lett.*, *85*, 277-288, 1987.

Clark, J. G., and J. Dymond, Geochronology and petrochemistry of Easter and Sala y Gomez Islands: Implications for the origin of the Sala y Gomez Ridge, *J. volcanol. Geotherm. Res.*, *2*, 29-48, 1977.

DeMets, C., R. G. Gordon, D. F. Argus, and S. Stein, Current plate motions, *Geophys. J. Int.*, *101*, 425-478, 1990.

Dorman, L. M., and B. T. R. Lewis, Experimental isostasy, 1, Theory of the determination of the Earth's isostatic response to a concentrated load, *J. Geophys. Res.*, *75*, 3357-3365, 1970.

Firth, R., *Pacific Islands*, 739pp, Oxford Univ. Press, New York, 1943.

Fisher, R. L. and R. M. Norris, Bathymetry and geology of Sala y Gomez, southeast Pacific, *Geol. Soc. Am. Bull*, *71*, 497-502, 1960.

Fontignie, D., and J.-G. Schilling, $^{87}Sr/^{86}Sr$ and REE variations along the Easter Microplate boundaries (South Pacific): Application of multivariate statistical analyses to ridge segmentation, *Chem. Geol.*, *89*, 209-241, 1991.

Forsyth, D. W., Subsurface loading and estimates of the flexural rigidity of continental lithosphere, *J. Geophys. Res.*, *90*, 12623-12632, 1985.

Gerlach, D. C., S. R. Hart, V. W. J. Morales, and C. Palacios, Mantle heterogeneity beneath the Nazca Plate: San Felix and Juan Fernandez islands, *Nature*, *322*, 165-169, 1986.

Gripp, A. E., Current plate motions: Reference frames and uncertainties, Ph.D. dissertation, Northwestern Univ., Evanston, Ill., 1994.

Haase, K. M., and C. W. Devey, Geochemistry of lavas from the Ahu and Tupa volcanic fields, Easter Hotspot, southeast Pacific: Implications for intraplate magma genesis near a spreading axis, *Earth Planet. Sci. Lett.*, *137*, 129-143, 1996.

Haase, K. M., C. W. Devey, and S. L. Goldstein, Two-way exchange between the Easter mantle plume and the Easter microplate spreading axis, *Nature*, *382*, 344-346, 1996.

Hagen, R. A., N. A. Baker, D. F. Naar, and R. N. Hey, A SeaMARC II survey of recent submarine volcanism near Easter Island, *Mar. Geophys. Res.*, *12*, 297-315, 1990.

Hanan, B. B. and J.-G. Schilling, Easter microplate evolution: Pb isotope evidence, *J. Geophys. Res.*, *94*, 7432-7448, 1989.

Herron, E. M., Sea-floor spreading and the Cenozoic history of the east-central Pacific, *Geol. Soc. Am. Bull.*, *83*, 1672-1692, 1972a.

Herron, E. M., Two small crustal plates in the South Pacific near Easter Island, *Nature*, *240*, 35-37, 1972b.

Hey, R. N., P. D. Johnson, F. Martinez, J. Korenaga, M. L. Somers, Q. J. Huggett, T. P. Lebas, R. I. Rusby, and D. F. Naar, Plate boundary reorganization along the fastest seafloor spreading center, *Nature*, *378*, 167-170, 1995.

Ihinger, P. D., Mantle flow beneath the Pacific plate: Evidence from seamount segments in the Hawaiian-Emperor Chain, *Am. J. Sci.*, *295*, 1035-1057, 1995.

Kingsley, R. H., J.-G. Schilling, R. Poreda, R. Batiza, D. Naar, and D. Fontignie, Easter Salas y Gomez Seamount Chain: PB isotope evidence (abstract), *Eos Trans. AGU*, *75(44)*, Fall Meet. Suppl., 726, 1994.

Liu, Z. J., The origin and evolution of the Easter Seamount Chain, Ph.D. thesis, Univ. of South Fla., Tampa, Fla., 1996.

Liu, Z. J., D. F. Naar, Y. Rappaport, S. E. Kruse, and R. N. Hey, Hot bubbles: Formation of the Easter Seamount Chain (abstract), *Eos, Trans. AGU*, *76(46)*, Fall Meet. Suppl., 586, 1995.

Lonsdale, P., Segmentation of the Pacific-Nazca spreading center, 1°N-20°S, *J. Geophys. Res.*, *94*, 12197-12225, 1989.

Louden, K. E., and D. W. Forsyth, Crustal structure and isostatic compensation near the Kane Fracture Zone from topography and gravity measurements, I, spectral analysis approach, *Geophys. J. R. Astron. Soc.*, *68*, 725-750, 1982.

Macario, A., A. Malinverno, and W. F. Haxby, On the robustness of elastic thickness estimates obtained using the coherence method, *J. Geophys. Res.*, *100*, 15163 - 15172, 1995.

McNutt, M., Implications of regional gravity for state of stress in the Earth's crust and upper mantle, *J. Geophys. Res.*, *85*, 6377-6396, 1980.

Menard, H. W., T. E. Chase, and S. M. Smith, Galapagos rise in the southeast Pacific, *Deep Sea Res. Oceanogr. Abstr.*, *11*, 233-242, 1964.

Minster, J. B. and T. H. Jordan, Present-day plate motions, *J. Geophys. Res.*, *83*, 5331-5354, 1978.

Morgan, W. J., Convection plumes in the lower mantle, *Nature*, *230*, 197-198, 1971.

Morgan, W. J., Rodriguez, Darwin, Amsterdam,..., A second type of hotspot Island, *J. Geophys. Res.*, *83*, 5355-5360, 1978.

Naar, D. F., and R. N. Hey, Speed limit for oceanic transform faults, *Geology*, *17*, 420-422, 1989.

Naar, D. F., and R. N. Hey, Tectonic evolution of the Easter microplate, *J. Geophys. Res.*, *96*, 7961-7993, 1991.

Naar, D. F., R. Batiza, R. Poreda, and J.-G. Schilling, Final cruise report for the R/V *Melville* Gloria Expedition legs 6 and 7 (report), 26,pp., NSF, 1993a.

Naar, D. F., et al., GLORI-B and geochemical investigation of the Easter Seamount Chain: EPR to San Ambrosio Island, *Eos, Trans., AGU*, 74, 672, 1993b.

National Oceanic and Atmospheric Administration (NOAA), ETOPO-5 bathymetry/topography data, Data Announc. 88-MGG-02, Nat. Geophy. Data Cent., Boulder, Colo., 1988.

O'Connor, J. M., P. Stoffers, and M. O. Mcwilliams, Time-space mapping of Easter Chain volcanism, *Earth Planet. Sci. Lett.*, *136*, 197-212, 1995.

Okal, E. A., and A. Cazenave, A model for the plate tectonic evolution of the east-central Pacific based on SEASAT investigations, *EPSL*, *72*, 99-116, 1985.

Parson, B., and J. G. Sclater, An analysis of the variation of ocean floor bathymetry and heat flow with age, *J. Geophys. Res.*, *82*, 803-827, 1977.

Pilger, R. H., Jr., and D. W. Handschumacher, The fixed-hotspot hypothesis and the origin of the Easter-Sala y Gomez-Nazca trace, *Geol. Soc. Am. Bull.*, *92*, 437-446, 1981.

Poreda, R. J., J.-G. Schilling, R. Batiza, and D. Naar, Helium isotope ratios in Easter microplate basalts, *Earth Planet. Sci. Lett.*, *119*, 319-329, 1993a.

Poreda, R. J., J.-G. Schilling, R. Batiza, and D. Naar, Geochemistry of Volcanism along the Easter Seamount Chain (abstract), *Eos Trans. AGU*, *74*(43), Fall Meet. Suppl., 672, 1993b.

Rusby, R. I., and R. C. Searle, A history of the Easter microplate, 5.25 Ma to present, *J. Geophys. Res.*, *100*, 12617-12640, 1995.

Sandwell, D. T., E. L. Winterer, J. Mammerickx, R. A. Duncan, M. A. Lynch, D. A. Levitt, and C. L. Johnson, Evidence for diffuse Extension of the Pacific plate from Pukapuka ridges and cross-grain gravity lineations, *J. Geophys. Res.*, *100*, 15087-15099, 1995.

Schilling, J.-G., Fluxes and excess temperatures of mantle plumes inferred from their interaction with migrating mid-ocean ridges, *Nature*, *352*, 397-403, 1991.

Schilling, J.-G., and A. Noe-Nygaard, Faeroe-Iceland plume: Rare-Earth evidence, *Earth Planet. Sci. Lett.*, *24*, 1-14, 1974.

Schilling, J.-G., H. Sigurdsson, A. N. Davis, and R. N. Hey, Easter microplate evolution, *Nature*, *317*, 325-331, 1985a.

Schilling, J.-G., G. Thompson, R. Kingsley, and S. Humphris, Hotspot-migrating ridge interaction in the South Atlantic, *Nature*, *313*, 187-191, 1985b.

Searle, R. C., J. Francheteau, and B. Cornaglia, New observations on mid-plate volcanism and the tectonic history of the Pacific Plate, Tahiti to Easter microplate, *Earth Planet. Sci. Lett.*, *131*, 395-421, 1995.

Smith, W. H. F., and D. T. Sandwell, Bathymetric prediction from dense satellite altimetry and sparse shipboard bathymetry, *J. Geophys. Res.*, *99*, 21803-21824, 1994.

Smith, W. H. F. and D. T. Sandwell, Marine gravity field from declassified Geosat and ERS-1 altimetry (abstract), *Eos Trans. AGU*, *76*(46), Fall Meet. Suppl., 156, 1995a.

Smith, W. H. F., and D. T. Sandwell, Oceanographic "pseudogravity" in marine gravity fields derived from declassified Geosat and ERS-1 altimetry (abstract), *Eos Trans. AGU*, *76*(46), Fall Meet. Suppl., 151, 1995b.

Stoffers, P., R. Hekinian, K. M. Haase, and Scientific Party, Geology of young submarine volcanoes west of Easter Island, southeast Pacific, *Mar. Geol.*, *118*, 177-185, 1994.

Wessel, P., Thermal stresses and the bimodal distribution of elastic thickness estimates of the oceanic lithosphere, *J. Geophys. Res.*, *97*, 14177-14193, 1992.

Wessel, P., and W. H. Smith, Free software helps map and display data, *Eos Trans. AGU*, *72*(41), 441, 445-446, 1991.

Wessel, P., and A.B. Watts, On the accuracy of marine gravity measurements, *J. Geophys. Res.*, *93*, 393-413, 1988.

Wilson, J. T., Evidence from islands on the spreading of ocean floors, *Nature*, *197*, 536-538, 1963a.

Wilson, J. T., A possible origin of the Hawaiian Islands, *Can. J. Phys.*, *41*, 863-870, 1963b.

Wilson, J. T., Convection currents and continental drift, *Philos. Trans. R. Soc. London, Ser. A*, *258*, 145-167, 1965.

Winterer, E. L., and D. T. Sandwell, Evidence from en-echelon cross-grain ridge tensional cracks in the Pacific plate, *Nature*, *329*, 534-537, 1987.

Wolfe, C. J., and M. K. McNutt, Compensation of Cretaceous seamounts of the Darwin Rise, northwest Pacific Ocean, *J. Geophys. Res.*, *96*, 2363-2373, 1991.

Woods, A., E. Plank, S. Kruse, D. F. Naar, and Z. J. Liu, Compensation of Seamounts along the Easter Seamount Chain (abstract), *Eos Trans. AGU*, *74*(43), Fall Meet. Suppl., 687, 1993.

Woods, M. T., and E. A. Okal, The structure of the Nazca Ridge and Sala y Gomez Seamount Chain from the dispersion of Rayleigh waves, *Geophys. J. Int.*, *117*, 205-222, 1994.

R. A. Duncan, College of Oceanic and Atmospheric Sciences, Oregon State University, Corvallis, OR 97331. (e-mail: rduncan@oce.orst.edu)

S. E. Kruse, Geology Department, University of South Florida, 4202 E. Fowler Avenue, Tampa, FL 33620. (e-mail: skruse@chuma.cas.usf.edu)

Z. J. Liu, Computer Science Department, Stanford University, Palo Alto, CA 94305. (e-mail: zjl@cs.stanford.edu)

D. F. Naar, Marine Science Department, University of South Florida, 140 Seventh Avenue South, St. Petersburg, FL 33701-5016. (e-mail: naar@marine.usf.edu)

(Received December 16, 1996; revised July 4, 1997; accepted July 28, 1997.)